Quantum tunneling in real space: Tautomerization of single porphycene molecules on the (111) surface of Cu, Ag, and Au

(article starts on next page)

Quantum tunneling in real space: Tautomerization of single porphycene molecules on the (111) surface of Cu, Ag, and Au

Takashi Kumagai,[1,a)] Janina N. Ladenthin,[1] Yair Litman,[2] Mariana Rossi,[2,a)] Leonhard Grill,[3] Sylwester Gawinkowski,[4] Jacek Waluk,[4,5] and Mats Persson[6,7]

[1]*Department of Physical Chemistry, Fritz-Haber Institute of the Max-Planck Society, Faradayweg 4-6, 14195 Berlin, Germany*
[2]*Theory Department, Fritz-Haber Institute of the Max-Planck Society, Faradayweg 4-6, 14195 Berlin, Germany*
[3]*Department of Physical Chemistry, University of Graz, Heinrichstrasse 28, 8010 Graz, Austria*
[4]*Institute of Physical Chemistry, Polish Academy of Sciences, Kasprzaka 44/52, Warsaw 01-224, Poland*
[5]*Faculty of Mathematics and Natural Sciences, College of Science, Cardinal Stefan Wyszyński University, Dewajtis 5, 01-815 Warsaw, Poland*
[6]*Surface Science Research Centre and Department of Chemistry, University of Liverpool, Liverpool L69 3BX, United Kingdom*
[7]*Department of Physics, Chalmers University of Technology, SE 41296 Göteborg, Sweden*

Tautomerization in single porphycene molecules is investigated on Cu(111), Ag(111), and Au(111) surfaces by a combination of low-temperature scanning tunneling microscopy (STM) experiments and density functional theory (DFT) calculations. It is revealed that the *trans* configuration is the thermodynamically stable form of porphycene on Cu(111) and Ag(111), whereas the *cis* configuration occurs as a meta-stable form. The *trans* → *cis* or *cis* → *trans* conversion on Cu(111) can be induced in an unidirectional fashion by injecting tunneling electrons from the STM tip or heating the surface, respectively. We find that the *cis* ↔ *cis* tautomerization on Cu(111) occurs spontaneously via tunneling, verified by the negligible temperature dependence of the tautomerization rate below ~23 K. Van der Waals corrected DFT calculations are used to characterize the adsorption structures of porphycene and to map the potential energy surface of the tautomerization on Cu(111). The calculated barriers are too high to be thermally overcome at cryogenic temperatures used in the experiment and zero-point energy corrections do not change this picture, leaving tunneling as the most likely mechanism. On Ag(111), the reversible *trans* ↔ *cis* conversion occurs spontaneously at 5 K and the *cis* ↔ *cis* tautomerization rate is much higher than on Cu(111), indicating a significantly smaller tautomerization barrier on Ag(111) due to the weaker interaction between porphycene and the surface compared to Cu(111). Additionally, the STM experiments and DFT calculations reveal that tautomerization on Cu(111) and Ag(111) occurs with migration of porphycene along the surface; thus, the translational motion couples with the tautomerization coordinate. On the other hand, the *trans* and *cis* configurations are not discernible in the STM image and no tautomerization is observed for porphycene on Au(111). The weak interaction of porphycene with Au(111) is closest to the gas-phase limit and therefore the absence of *trans* and *cis* configurations in the STM images is explained either by the rapid tautomerization rate or the similar character of the molecular frontier orbitals of the *trans* and *cis* configurations. © 2017 Author(s). All article content, except where otherwise noted, is licensed under a Creative Commons Attribution (CC BY) license (*http://creativecommons.org/licenses/by/4.0/*). https://doi.org/10.1063/1.5004602

INTRODUCTION

Quantum tunneling of H atoms (or protons) was recognized already at the dawn of quantum chemistry[1] and found to play a significant role in important chemical and biological reactions.[2–4] Coherent tunneling in H-bond rearrangement and H-atom transfer reactions has been studied extensively by means of high-resolution rotational–vibrational and electronic spectroscopies in which tunneling is manifested as splitting of rotational/vibrational levels.[5,6] Intramolecular H-atom transfer reactions, the so-called tautomerization, in

organic molecules have served as an important model for studying hydrogen dynamics.[7] For instance, tautomerization of malonaldehyde[8–13] and tropolone[14–20] has been intensely investigated by spectroscopic experiments and quantum chemical calculations. These studies revealed that relatively heavy atoms (e.g., carbon or oxygen) in the molecular frame also contribute to the tunneling process.

Recently, low-temperature scanning tunneling microscopy (STM) has been used to observe directly single-molecule tautomerization in porphyrin and phthalocyanine derivatives on surfaces.[21–25] Particularly, porphycene, the first synthesized structural isomer of porphyrin,[26] has emerged as a fascinating model of intramolecular H bonding and a double H-atom transfer.[27,28] Due to the strong H bonds in the molecular

a)Authors to whom correspondence should be addressed: kuma@fhi-berlin.mpg.de and rossi@fhi-berlin.mpg.de

cavity,[29] the energy barrier of tautomerization in porphycene is relatively small, leading to a fast tautomerization rate[30,31] and a considerable contribution of hydrogen tunneling.[32–34] Recently, we have demonstrated that tautomerization in a single porphycene molecule can be induced by various stimuli, namely heat, electrons, light, and chemical force.[35–39] These studies not only revealed the microscopic reaction mechanisms but also highlighted that adsorption of porphycene on a surface results in additional complexities in the tautomerization dynamics, caused by the interaction between the molecule and the surface as well as symmetry lowering due to the adsorption. Moreover, low-temperature STM has also been used to probe directly tunneling dynamics of H-atom diffusion,[40] H-bond rearrangement in small water clusters,[41,42] and tautomerization,[43] and the zero-point energy contribution in the H bond.[44,45] Interestingly, tunneling of heavy atoms or molecules was also observed for Cu,[46] Co,[47] and CO[48] on a Cu(111) surface at cryogenic temperatures. One of the unique capabilities of a low-temperature STM is to manipulate the potential landscape of adsorbate reactions by modifying a local environment of the molecule,[36,37] which enables us to control precisely tunneling dynamics.[42,43] Another, yet almost unknown, influence on the hydrogen tunneling results from the surface. Here we present a study on the tunneling dynamics of tautomerization in single porphycene molecules on different noble metals, namely Cu(111), Ag(111), and Au(111), by a combination of STM experiments and DFT calculations.

METHODS

All experiments were performed in an ultra-high vacuum chamber (base pressure of 10^{-10} mbar), equipped with a low-temperature STM (modified Omicron instrument with Nanonis Electronics). All STM images were acquired in the constant-current mode. The bias voltage was applied to either the tip (V_t) or sample (V_s), and all voltages are indicated as the sample bias V_s ($=-V_t$). The Cu(111), Ag(111), and Au(111) surfaces were cleaned by repeated cycles of argon ion sputtering and annealing. The STM tip was made from a W or PtIr wire and optimized *in situ* by applying a voltage pulse and poking the tip apex into the surface in a controlled manner. Porphycene molecules were deposited onto the surface at room temperature from a Knudsen cell (at 450–500 K).

The geometric structures and the minimum energy paths (MEPs) of the adsorbed porphycene molecule on the Cu(111) and Ag(111) surfaces were obtained from van der Waals corrected DFT calculations using FHI-aims[49] and the Vienna *ab initio* simulation program (VASP).[50] In the VASP calculations, the electron–ion core interactions and the exchange–correlation effects were treated using the Projector Augmented Wave (PAW) method[51] and the optB86b and vdW-DF-cx versions of the van der Waals density functional,[52–55] respectively. The Cu(111) surfaces were represented in a supercell by a four-layer slab with a (6 × 6) surface unit cell with a 20 Å vacuum region and by using 3 × 3 × 1 k-grids. In the simulations performed with FHI-aims, we used the PBE functional augmented with van der Waals interactions tailored for surface adsorption (PBE+vdW^{surf})[56] (unless specified otherwise), where we ignored the vdW contribution for pairs of metallic atoms, used tight settings for numerical grids and basis sets, a 6 × 6 surface including 4 metallic layers, a vacuum separation of 60 Å, and a k-grid of 12 × 12 × 1 for Cu(111) and 14 × 14 × 1 for Ag(111). In all calculations, we have employed a dipole correction in order to optimally decouple periodic images.[57] The MEPs were computed with the nudged elastic band method and the string method.[58,59] STM images were simulated considering a 0.2 eV window below the Fermi level with the Tersoff-Hamann model.[60,61]
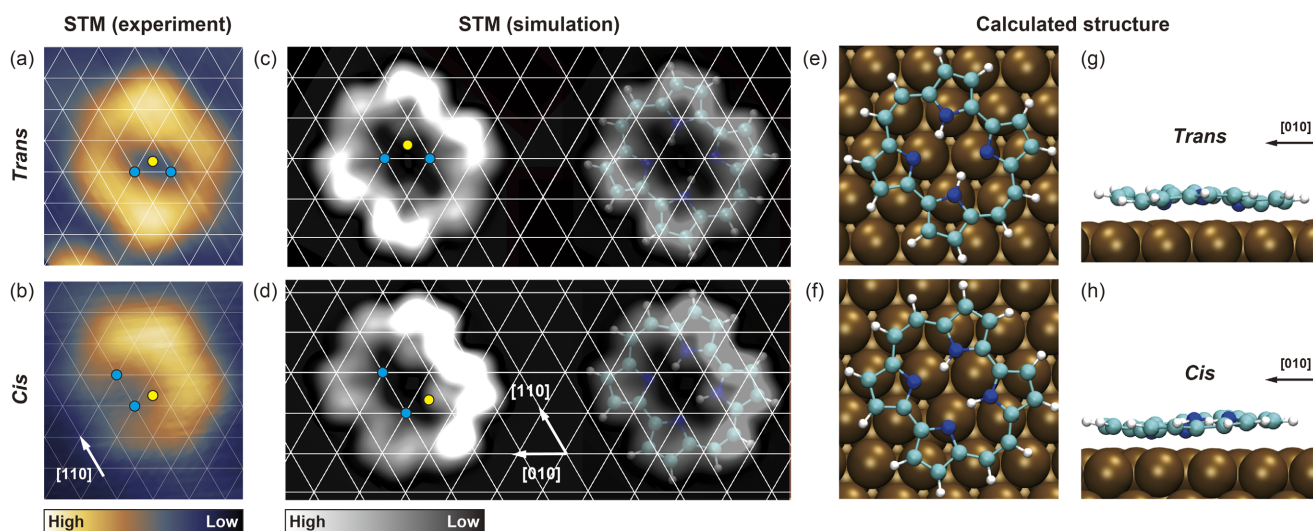

FIG. 1. Porphycene on Cu(111). [(a) and (b)] STM images of a single porphycene on Cu(111) at 5 K in the *trans* and *cis* configurations ($V_s = -50$ mV, $I_t = 5$ nA for (a) and 10 nA for (b), 1.4×1.5 nm^2). The color scale corresponds to the apparent height from −10 to 75 pm. [(c) and (d)] Simulated STM images. The white grid lines represent the surface lattice of Cu(111). On the right side, we superimpose the simulated STM images with the calculated structures. The yellow dots in (a)–(d) indicate a hollow site in order to serve as a guide to the eye for the small displacement of the molecule before and after tautomerization. The blue dots in (a)–(d) indicate the nearest on-top site of the surface Cu atoms to which the imine N atoms are bonded. [(e)–(h)] Top and side view of the optimized structures.

RESULTS AND DISCUSSION

Figures 1(a) and 1(b) show an STM image of a single porphycene molecule on Cu(111) at 5 K in the *trans* and *cis* configurations, respectively. The surface lattice underneath the molecule (white grid lines) is determined from atomic-resolution images using the point contact method with a Cu adatom[47,62] (see the supplementary material, Fig. S1). The *trans* configuration is the thermodynamically stable form, whereas the *cis* configuration occurs as a meta-stable form.[37,38] A *trans* porphycene can be converted to the *cis* configuration in an unidirectional fashion either by injecting tunneling electrons from the STM[37] or photo-excitation,[38] whereas the backward *cis → trans* tautomerization can be induced by heating the surface and all *cis* molecules are converted to the *trans* configuration above ~35 K. Although the *cis ↔ cis* tautomerization also occurs (cf. Fig. 3), no *trans ↔ trans* conversion was observed. The STM images [Figs. 1(a) and 1(b)] suggest a slight migration of porphycene upon the *trans → cis* tautomerization (see also the supplementary material, Fig. S2), which is estimated to be 0.7(±0.3) Å along the high-symmetry axis, e.g., the [110] direction, of Cu(111). Figures 1(c)–1(h) display the simulated STM images and the optimized structures on Cu(111). We have performed an exhaustive grid search of possible geometries of the *trans* and *cis* tautomers on Cu(111), by translating the center of mass and rotating the structures. Since porphycene can adopt distorted geometries on the surface, we found several minima that differ by slight rotations and buckling of the molecule, which differ by up to 0.1 eV in energy. In the following, we discuss only the lowest-energy structures. The optimized structures [Figs. 1(e) and 1(f)] reveal that the *trans* and *cis* porphycene adsorb on a different site with a relative displacement of about 0.7 Å, which is in good agreement with the migration distance observed in the experiment [Figs. 1(a) and 1(b)]. We discuss the adsorption site in terms of the character of the hollow or bridge site closest to the center of mass of the molecule. The theoretical STM images in Figs. 1(c) and 1(d) show remarkable agreement with the experiments. The calculated structures show a deformation of the macrocycle of porphycene [Figs. 1(g) and 1(h)], which is planar in the gas phase. The distortion can be attributed to the stronger interaction of the imine N atoms with the surface Cu atoms underneath. The simulated charge density differences (Fig. 2) indicate that the density rearrangement between the imine N atoms and the surface Cu atoms is larger than that for the amine groups. This deformation of the macrocycle leads to weakening of the inner H bonds, which is manifested as a significant blue-shift of the calculated harmonic frequencies of the symmetric and anti-symmetric N–H stretches compared to the gas-phase (Table I). Additionally, a Hirshfeld analysis[63] indicates that both tautomers of porphycene on Cu(111) are negatively charged with about 0.5*e*. This charging is in line with the experimental observation that porphycene does not aggregate spontaneously on the surface and no island formation occurs at low coverage.[37]

Overall, experimental and theoretical results appear to be consistent within the expected error bars of around 10 meV in calculated energy differences. With the functionals used, we find the *trans* isomer to be isoenergetic or slightly lower in energy than the *cis* tautomer (Table II). Recently, Novko
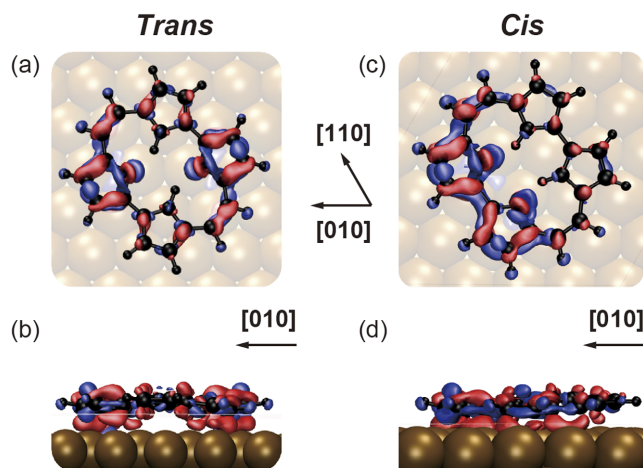

FIG. 2. Charge density differences of porphycene on Cu(111), which is defined by $\Delta\rho = \rho_{\text{porphycene/Cu}} - \rho_{\text{porphycene}} - \rho_{\text{Cu}}$ with $\rho_{\text{porphycene/Cu}}$, $\rho_{\text{porphycene}}$, and ρ_{Cu} being the charge densities of the porphycene–Cu(111) system, the isolated porphycene, and the Cu(111) surface, respectively. Red and blue represent the isosurfaces at $+0.015e/\text{Å}^3$ (charge accumulation) and $-0.015e/\text{Å}^3$ (charge depletion), respectively.

et al. showed that the treatment of dispersion interactions and the choice of exchange–correlation functionals could play a role to determine the relative stability between the *trans* and *cis* configurations of porphycene on Cu(111).[64,65] However, they did not take into account the migration of porphycene upon the tautomerization as described above. Our calculations show that placing a *trans* tautomer on the hollow (hcp) site (the preferred site for the *cis* tautomer) results in a spontaneous migration (barrierless) from the hollow site to the bridge site [Fig. 1(e)] when relaxation is allowed. For the *cis ↔ cis* tautomerization, we also find that porphycene moves from the hcp to the fcc site spontaneously, thus this process is also barrierless.

Figures 3(a) and 3(b) show STM images of a *cis* porphycene before and after one *cis → cis* tautomerization event. The tautomerization can be induced either by injecting energetic electrons from the STM[37] or photo-irradiation.[38] Additionally, we find that the *cis ↔ cis* tautomerization also occurs spontaneously even at 5 K, although the rate is much smaller than that of the STM- or photo-induced processes. By comparing the position of porphycene relative to the Cu adatom nearby, it is revealed that porphycene moves upon the tautomerization. The migration direction is governed by the molecular orientation; it takes place along one of the high-symmetry axes of Cu(111) which follows the long axis of porphycene, and no rotation of porphycene was observed. The calculated structure provides atomistic insight into the migration. As discussed above, the imine N atoms in the *cis*

TABLE I. Calculated symmetric (anti-symmetric) N–H stretching frequencies of porphycene. The structure of the gas phase molecule was relaxed.

	Frequency (cm^{-1})
cis (hcp) on Cu(111)[a]	2968 (2912)
cis in gas phase	2283 (2243)
trans on Cu(111)	3058 (3072)
trans in gas phase	2591 (2582)

[a]The same frequency is obtained on the fcc site.

TABLE II. Summary of the calculated energy differences (ΔE) and the relative displacement (Δd) of porphycene on Cu(111) with respect to the *cis* (hcp) structure for each functional. E_{ZPE} represents the zero-point corrected energy. Δd is defined as the displacement of the center-of-mass of the N atoms.

	cis (fcc)			*trans*		
	PBE+vdW^{surf} (FHI-aims)	optB86b-vdW (VASP)	vdW-DF-cx (VASP)	PBE+vdW^{surf} (FHI-aims)	optB86b-vdW (VASP)	vdW-DF-cx (VASP)
ΔE (meV)	7	−7	10	3	28	−23
E_{ZPE} (meV)	7			5		
Δd (Å)	1.40	1.21	1.21	0.71	0.74	0.74

porphycene are strongly bound to the surface Cu atoms underneath [Figs. 2(c) and 2(d)]. The translation of the molecule by ~1.4 Å ($\approx \frac{a_0}{2\sqrt{2}}$) (along the [110] axis) makes it possible for the newly formed imine N atoms to resume a similar bonding geometry with the Cu atoms. It should also be noted that the translation results in a change of the adsorption position of porphycene, i.e., between the hcp and fcc sites of Cu(111). Porphycene at the hcp site is only 7 meV more stable than at the fcc site (Table II) in our calculations, including zero-point energies (ZPEs). In experiment we were not able to discriminate between the porphycene molecules at the fcc or hcp site in the STM image. However, a possible difference resulting from the fcc or hcp site is observed in the tautomerization rate (as discussed below), which indicates that the calculated energy difference between the *cis* tautomers on the fcc and hcp sites may be real. Our calculations also find that the *trans–trans* tautomerization without any translational motion of the molecule results in an increase of the total energy by more than 0.15 eV with respect to the optimized geometry; thus, the process should occur via the *cis* configuration.

Figure 4(a) shows the current dependence of the *cis* ↔ *cis* tautomerization rate obtained at different bias voltages. At 170 mV, tunneling electrons trigger the reaction through vibrational excitation via an inelastic electron tunneling process.[37] The rate increases linearly with increasing current, indicating that the reaction proceeds via a single-electron process. Additionally, a possible difference between the *cis*(hcp) → *cis*(fcc) and *cis*(fcc) → *cis*(hcp) tautomerization is observed. The upward and downward triangles in Fig. 4(a) represent the rate determined for odd- and even-numbered *cis* → *cis* tautomerization events, respectively. With this analysis, a possible difference in the tautomerization rate from the hcp to fcc site and *vice versa* may appear since every *cis* → *cis* tautomerization event changes the adsorption site. We find, in this experiment, a higher tautomerization rate for the even-numbered events than that for the odd-numbered ones. According to the calculations, the *cis* configuration at the hcp site is slightly more favorable than that at the fcc site. Therefore, the even-numbered events may be assigned to the *cis*(fcc) → *cis*(hcp) transition. On the other hand, the rate obtained at a bias voltage of −50 mV shows only a rather weak dependence on the current [Fig. 4(a)], indicating that the tautomerization is not induced by the tunneling electron and besides the influence of an electric field and tip–molecule interactions also plays a minor role. The tautomerization rate is also not significantly affected at a voltage of −10 mV. Note that the tautomerization rate shows a similar dependence at both bias polarities.[37,38] Because tautomerization occurs much less frequently at −50 mV, we obtained the rate by monitoring approximately 100 molecules in the
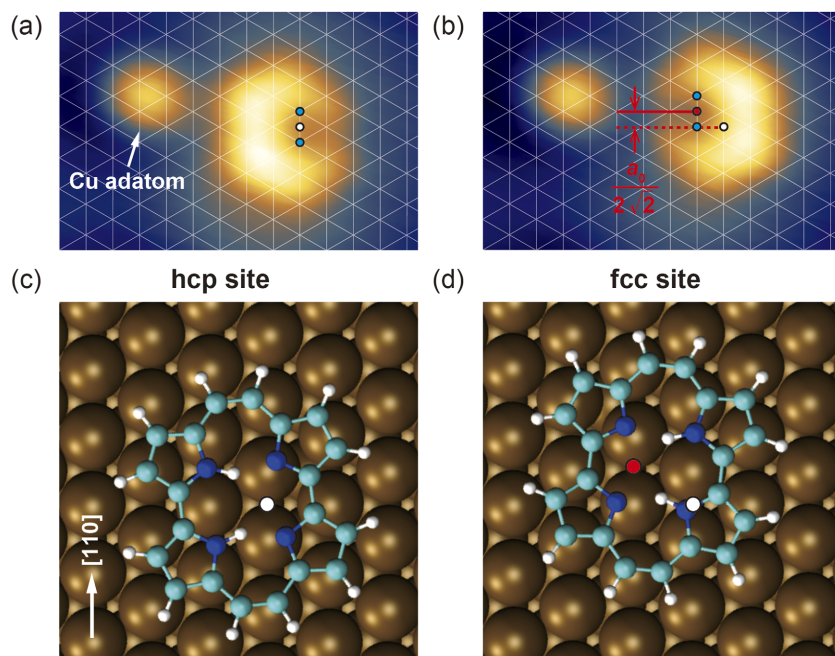

(a) Cu adatom
(b)
(c) **hcp site**
(d) **fcc site**
[110]

FIG. 3. *Cis* ↔ *Cis* tautomerization on Cu(111). [(a) and (b)] STM image of a single porphycene molecule before and after one tautomerization event at 5 K. The white grid lines represent the surface lattice of Cu(111). A single Cu adatom is placed near the molecule. The blue dots indicate the nearest on-top site of the surface Cu atoms to which the imine N atoms are bound. [(c) and (d)] Optimized structures of porphycene at the hcp and fcc sites, respectively. The white and red dots indicate the bridge site in between the imine N atoms before and after tautomerization, respectively.
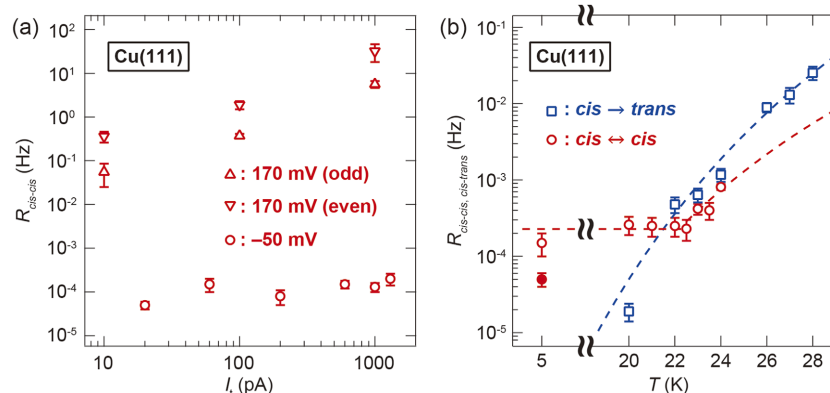
FIG. 4. *Cis ↔ Cis* tautomerization rate on Cu(111). (a) Current dependence of the rate obtained at 5 K and at V_s = 170 mV (triangles) and V_s = −50 mV (circles). The upward and downward triangles represent the rate obtained for odd- and even-numbered *cis → cis* tautomerization events, respectively. (b) Temperature dependence of the rate for the *cis ↔ cis* (red circles) and *cis → trans* (blue squares) conversion. The filled circle at 5 K shows the rate obtained under the tip conditions that result in a significant variation. The tautomerization rates were measured at bias voltage and tunneling current below or equal to 50 mV and 60 pA.

consecutive STM images and sampling all the events (see the supplementary material). Hence, a possible difference in the tautomerization rate between the *cis*(fcc) and *cis*(hcp) molecules was not considered. This procedure provides the average rate between the *cis*(fcc) → *cis*(hcp) and the opposite processes. Importantly, the tautomerization rate at −50 mV shows a rather weak dependence on the temperature below ~23 K [Fig. 4(b)], indicating that the process is governed by quantum tunneling. Note that the tautomerization rate appears to be significantly affected by the tip conditions. For instance, the use of a different tip or strong *in situ* tip forming procedure such as application of a voltage pulse and controlled indentation of the tip into the surface results in variation of the rate [data obtained with different tip conditions at 5 K are shown in Fig. 4(b)]. As we have demonstrated recently, the interaction between an STM tip and porphycene can modify the potential energy surface of the tautomerization.[39] Such a modification of potential energy surface may have a crucial impact particularly on the tunneling process. However, the lack of detailed knowledge of the tip apex structure hampers further quantitative description. A similar tip-to-tip variation was also observed for the *cis ↔ cis* tautomerization via tunneling on Ag(110).[43] The different behavior below and above ~23 K could be traced to a different H-atom transfer mechanism. For example, our DFT calculations find that a translational mode of the molecule starts being thermally excited at around 25 K, which would add a thermally activated contribution to tautomerization. However, the *cis → trans* conversion does depend on temperature even below 23 K, indicating a different mechanism, likely through thermally assisted tunneling.

It is evident that the *cis ↔ cis* tautomerization is coupled with the translational coordinate of porphycene along the surface (cf. Fig. 3). Additionally, the tautomerization can occur either in a stepwise or concerted fashion. In the former case, individual H atoms move separately and the reaction proceeds through a *trans* configuration. In the latter case, the H atoms are transferred collectively. Figure 5 displays the two-dimensional potential energy surface calculated for the stepwise *cis ↔ cis* tautomerization, where the vertical and horizontal axes correspond to the coordinate of the translational motion of

the molecule and the H-atom transfer, respectively. We only calculated the points marked with a cross in Fig. 5 and the others were obtained by an interpolation with cubic splines so that Fig. 5 should be taken as a qualitative representation of the potential energy surface. These energies do not include any ZPEs. We find that at this level, the stepwise pathway is energetically more favorable than the concerted one, with barriers along the minimum energy path of 76 meV for *cis–trans* and 135 meV for *cis–cis* (PBE+vdW^surf). The potential energy surface also reveals that the double H-atom transfer without migration of the molecule (path along the black arrow in Fig. 5) is not feasible because of a large activation barrier (369 meV). The *trans* configuration along the MEP is the same as the optimized structure in Fig. 1(e). However, in experiment, the *trans* configuration was not observed as a transient state during the *cis ↔ cis* tautomerization, and in addition, the *cis → trans* conversion rate is much smaller below about 23 K [Fig. 4(b)] and not observed at 5 K. The experimental results indicate that the *cis ↔ cis* tautomerization is governed by tunneling at low temperatures. However, a full evaluation of this path including ZPE

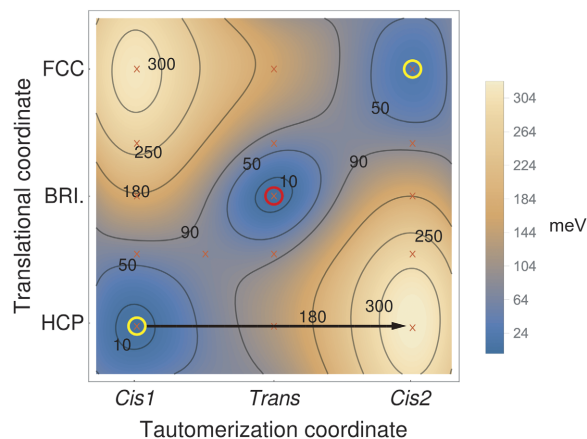

FIG. 5. Calculated potential energy surface of the *cis ↔ cis* tautomerization. The yellow and red circles represent the *cis* and *trans* configurations, respectively. The black arrow represents the double H-atom transfer without migration of the molecule. Red crosses represent calculated points on the potential energy surface.
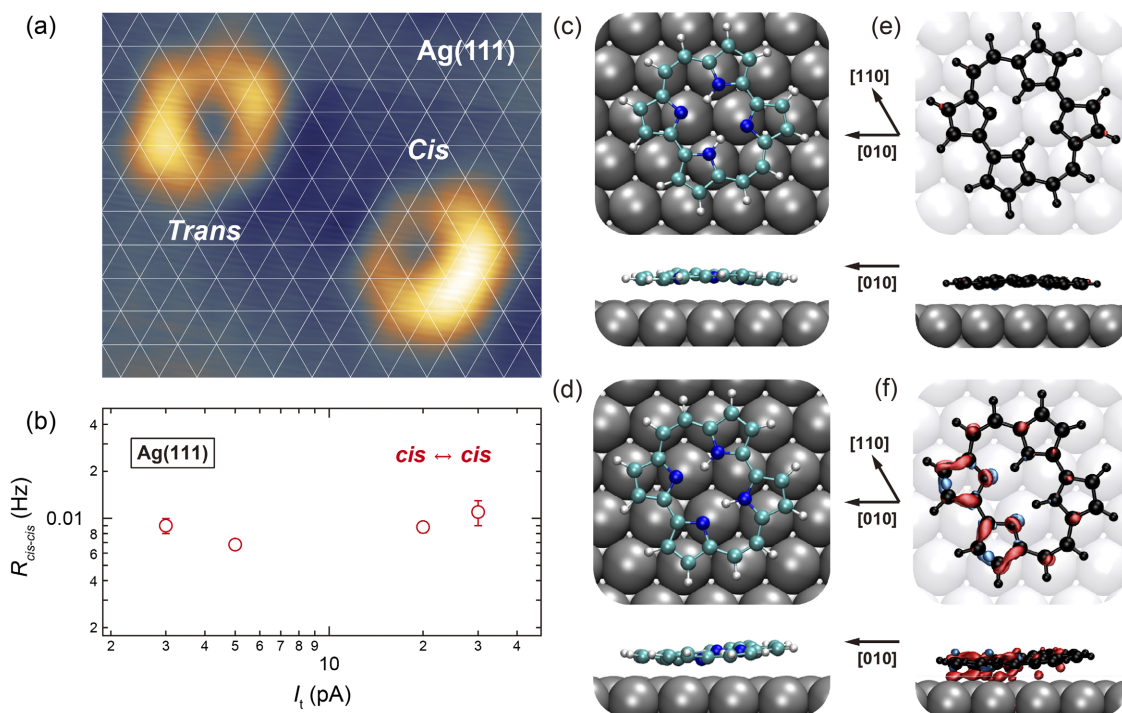
FIG. 6. Porphycene on Ag(111). (a) STM image of single porphycene molecules in the *trans* and *cis* configurations (5 K, V_s = 20 mV, I_t = 50 pA, 3.3 × 2.7 nm²). (b) Current dependence of the *cis* ↔ *cis* tautomerization rate measured at 5 K and V_s = 20 mV and I_t = 5 pA. [(c) and (d)] Optimized structures for the *trans* and *cis* (hcp) configurations, respectively. [(e) and (f)] Charge density difference of porphycene in the *trans* and *cis* (hcp) configurations, respectively. Red and blue represent the isosurfaces at +0.015e/Å³ (charge accumulation) and −0.015e/Å³ (charge depletion), respectively.

and tunneling, e.g., with path-integral molecular dynamics simulation, is beyond the scope of this work.

The tautomerization rate via tunneling is largely reduced for porphycene on the Cu(111) surface compared to the isolated molecule, e.g., 6×10^{11} Hz for the *trans* ↔ *trans* tautomerization determined from the tunneling splitting of 4.4 cm⁻¹ in the vibronic levels of the ground state.[33] This reduction of the rate can be explained by the increase of the tautomerization barrier compared to the isolated porphycene in inert media (estimated to be ~23 meV[30]). Additionally, the translational motion of porphycene during tautomerization on the surface leads not only to an increase of the path length and barrier but also to participation of other relatively heavy atoms (C and N atoms) in the reaction, giving rise to a further reduction of the tunneling rate.

Porphycene was also investigated on a Ag(111) surface. The STM appearance and adsorption geometries are similar to those on Cu(111) [Fig. 6(a)]. However, tautomerization between the *trans* and *cis* configurations also occurs spontaneously even at 5 K as well as the *cis* ↔ *cis* tautomerization with the latter being much more frequent. The resident time of

the *trans* tautomer is significantly longer than of the *cis* tautomer. Therefore, the former appears to be the thermodynamically stable form. Although a direct *trans* ↔ *trans* conversion event was rarely observed, we note that this might be attributed to the limited time resolution of the STM and the process could actually happen via the *cis* configuration. The displacement of porphycene is also observed in these tautomerizations (supplementary material, Fig. S4). The *cis* ↔ *cis* tautomerization rate on Ag(111) is obtained to be about 0.01 Hz at 5 K and does not depend on the tunneling current [Fig. 6(b)], suggesting that the process is governed by tunneling. It should be noted that the rate may be affected by tip conditions. The tautomerization rate on Ag(111) is about two orders of magnitude higher than on Cu(111). This suggests a smaller tautomerization barrier due to the weaker interaction of porphycene with the Ag(111) surface. Our calculations reveal that the *trans* and *cis* configurations on Ag(111) are essentially isoenergetic, with the *trans* configuration being only 4 meV more stable than *cis*

TABLE III. Summary of the calculated energy (E) of porphycene on Ag(111) given with respect to the *cis*-1 (fcc) structure. In *cis*-2 (fcc), two inner H atoms are transferred. In *trans*-1, one inner H atom of *cis*-1 (fcc) is transferred and the system is relaxed. In *trans*-2, *trans*-1 is displaced to the similar geometry with the *trans* configuration on Cu(111). The calculations were done using FHI-aims.

Structure	*cis*-1 (fcc)	*cis*-2 (fcc)	*cis*-2 (hcp)	*trans*-1	*trans*-2
E (meV)	0	152	8	36	−4

TABLE IV. Summary of the porphycene–surface distance measured through the average height of the amine (h_{amine}) and imine groups (h_{imine}) in each structure. The distance is given by the average height of the N atoms from the ion cores of the surface Cu atoms for each group. Differences in height (Δh) between h_{amine} and h_{imine} relate to the buckling of the structure. The binding energies with the PBE+vdW^{surf} functional, taking as a reference the molecules in the gas-phase (E_{bind}) are also listed.

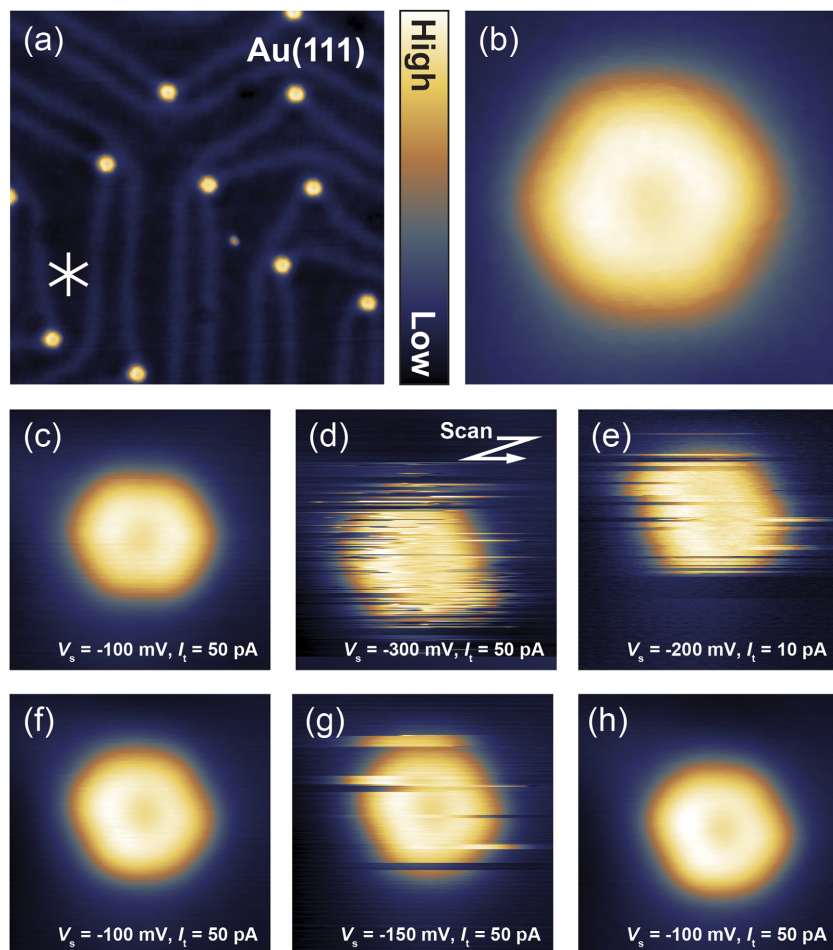|	h_{amine} (Å)	h_{imine} (Å)	Δh (Å)	E_{bind} (eV)
cis on Cu(111)	2.74	2.14	0.60	−4.0
trans on Cu(111)	2.53	2.23	0.30	−3.9
cis-1 on Ag(111)	3.02	2.52	0.50	−3.0
trans-2 on Ag(111)	3.08	2.98	0.10	−2.9

FIG. 7. Porphycene on Au(111). (a) STM image of porphycene molecules on Au(111) (5 K, $V_s = -100$ mV, $I_t = 20$ pA, 20×20 nm^2). The three white lines represent the high-symmetry axis of the Au(111) surface. (b) Enlarged STM image of a single porphycene molecule (5 K, $V_s = -50$ mV, $I_t = 20$ pA, 2×2 nm^2). [(c)–(h)] Sequential STM images of the same porphycene molecule recorded under different tunneling conditions (indicated in the figure). The scanning direction is indicated in (d). The image size is 2.5×2.5 nm^2.

(Table III). However, the translation from hcp to bridge site in the *cis–trans* tautomerization and from hcp to fcc site in the *cis–cis* tautomerization, observed for porphycene on Cu(111), does not happen spontaneously on Ag(111) due to a very low barrier in our calculation. Table IV summarizes the porphycene–surface distance, buckling of the molecule, and calculated binding energies taking as a reference the molecule in the gas-phase. The buckling of the *cis* porphycene is smaller on Ag(111) than Cu(111) due to a weaker interaction of the molecule with the surface atoms, which is also reflected in the larger molecule–surface distance on Ag(111). Additionally, the calculations indicate a significantly smaller charge density rearrangement of porphycene on Ag(111) [Figs. 6(e) and 6(f)] as compared to Cu(111) (Fig. 2), corroborating the relatively weak interaction of the molecule with Ag(111). Therefore, the potential energy surface of tautomerizations on Ag(111) is expected to be less corrugated than that on Cu(111), which rationalizes the much higher tautomerization rates observed in the experiment on Ag(111) than on Cu(111).

Porphycene was also investigated on the Au(111) surface where the molecules rapidly diffuse even at 5 K and under very low voltage and current conditions, like $V_s = 10$ mV, $I_t = 1$ pA. This rapid diffusion suggests a weaker interaction of porphycene with the Au(111) surface compared to Cu(111) and Ag(111). However, stationary molecules can be found at elbow sites of the herringbone reconstruction of Au(111) [Fig. 7(a)]. Unlike for porphycene on Cu(111) and Ag(111),

the *trans* and *cis* tautomers are indistinguishable in the STM image [Fig. 7(b)] and no evidence of a possible tautomerization was observed. The hopping and rotation of porphycene at the elbow site can be induced when the bias voltage is increased [Figs. 7(c)–7(h)]. However, the STM appearance does not change significantly upon hopping and rotation. The absence of any discernible *trans* or *cis* configuration suggests that either the tautomerization rate is much faster than the time-resolution of the STM (hundreds of microseconds) or the molecular orbitals of *trans* and *cis* cannot be distinguished. Our DFT calculations reveal that the frontier orbitals of *trans* and *cis* tautomers in the gas-phase appear to be similar (see the supplementary material, Fig. S5), and the weak interaction between the molecule and Au(111) is close to the gas-phase limit, making these tautomers indistinguishable in the STM image.

CONCLUSION

Single porphycene molecules were investigated on Cu(111), Ag(111), and Au(111) surfaces by using low-temperature STM. We find a correlation of the adsorption structure and tautomerization dynamics with the interaction strength between porphycene and the surfaces. On Cu(111) and Ag(111), the *trans* configuration is found to be the thermodynamically stable form, whereas the *cis* configuration occurs as the meta-stable form. On Cu(111), the *cis* ↔ *cis*

tautomerization occurs spontaneously even at low bias voltages (<50 mV) and the tautomerization rate is temperature independent at low temperatures, indicating that the process is governed by quantum tunneling. However, on Ag(111), the *cis* ↔ *cis* tautomerization rate is much greater than on Cu(111) and *trans* ↔ *cis* tautomerization occurs spontaneously at 5 K, indicating smaller potential barriers for the tautomerization on Ag(111) than on Cu(111) because of the weaker porphycene–surface interaction. Additionally, it is also found that the tautomerization of porphycene on Cu(111) and Ag(111) occurs with a migration of the molecule along the surface. This indicates that the translational motion of porphycene couples with the tautomerization coordinate. The adsorption geometries of porphycene were obtained on the Cu(111) and Ag(111) surfaces by using van der Waals corrected DFT calculations. The calculated structures revealed that the porphycene macrocycle, which is planar in the gas phase, is deformed on both surfaces due to the interaction of the molecule with the surface atoms. This distortion is smaller on Ag(111) than on Cu(111), which points to a weaker interaction of porphycene with Ag(111) than with Cu(111), corroborated by smaller charge density rearrangement of the molecule on the former. The two-dimensional potential energy surface of the tautomerization was also examined on Cu(111). Our calculations predict that the translational motion of porphycene upon tautomerization and the calculated barriers for all tautomerization processes are too high to be overcome at cryogenic temperatures used in the experiment. Zero-point energy corrections to the minimum energy structures do not change the potential energy landscape. This observation, together with the experimental results, suggests that the tautomerization proceeds predominantly by tunneling. Indeed, in our current calculation that does not include nuclear quantum effects, we predict that the *cis* ↔ *cis* tautomerization would likely happen through a stepwise mechanism, which was not observed experimentally. The multidimensional nature of this tunneling process calls for a high-level theoretical treatment of the inclusion of tunneling in the reaction rates, which is a natural next step for this work. Finally, on the Au(111) surface, it is not possible to discern *trans* and *cis* tautomers by the STM images and thus no tautomerization rate could be extracted. This observation may suggest that the tautomerization rate is much faster than the time resolution of the STM or that due to the similarity of the frontier molecular orbitals of the *trans* and *cis* configurations in the gas-phase, these tautomers may become indistinguishable for the STM when the interaction with the surface is very weak.

SUPPLEMENTARY MATERIAL

See supplementary material for (1) adsorption geometry analysis of porphycene on Cu(111) using point contact imaging with a Cu adatom, (2) migration of porphycene upon *trans* → *cis* tautomerization on Cu(111), (3) analysis of the *cis* ↔ *cis* tautomerization rate on Cu(111) at V_s = 170 mV, (4) analysis of the *cis* ↔ *cis* tautomerization rate on Cu(111) at low voltages and temperatures, (5) analysis of the *cis* → *trans* and *cis* ↔ *cis* tautomerization rate on Cu(111) at elevated temperatures, (6) migration of porphycene upon tautomerization on Ag(111), (7) analysis of the *cis* ↔ *cis* tautomerization rate on Ag(111), and (8) images of HOMO and LUMO of *trans* and *cis* porphycene in the gas-phase. We also provide the geometries of the *cis* and *trans* isomers of porphycene on Cu(111) optimized with the PBE+vdW^{surf} functional used in this work.

[1] R. P. Bell, *The Tunnel Effect in Chemistry* (Chapman & Hall, London, 1980).

[2] R. J. McMahon, "Chemical reactions involving quantum tunnelling," Science **299**, 833–834 (2003).

[3] R. J. Shannon, M. A. Blitz, A. Goddard, and D. E. Heard, "Accelerated chemistry in the reaction between the hydroxyl radical and methanol at interstellar temperatures facilitated by tunnelling," Nat. Chem. **5**, 745–749 (2013).

[4] J. P. Klinman and A. Kohen, "Hydrogen tunnelling links protein dynamics to enzyme catalysis," Annu. Rev. Biochem. **82**, 471–496 (2013).

[5] R. C. Cohen and R. J. Saykally, "Vibration-rotation-tunneling spectroscopy of the van der Waals bond: A new look at intermolecular forces," J. Phys. Chem. **96**, 1024–1040 (1992).

[6] Ö. Birer and M. Havenith, "High-resolution infrared spectroscopy of the formic acid dimer," Annu. Rev. Phys. Chem. **60**, 263–275 (2009).

[7] *Tautomerism*, edited by L. Antonov (Weiley-VHC, 2013).

[8] W. F. Rowe, Jr., R. W. Duerst, and E. Bright Wilson, "The intramolecular hydrogen bond in malonaldehyde," J. Am. Chem. Soc. **98**, 4021–4023 (1976); S. L. Baughcum, R. W. Duerst, W. F. Rowe, Z. Smith, and E. Bright Wilson, "Microwave spectroscopic study of malonaldehyde (3-hydroxy-2-propenal). 2. Structure, dipole moment, and tunneling," *ibid.* **103**, 6296–6303 (1981).

[9] T. Carrington, Jr. and W. H. Miller, "Reaction surface description of intramolecular hydrogen atom transfer in malonaldehyde," J. Chem. Phys. **84**, 4364–4370 (1986).

[10] N. Shida, P. F. Barbara, and J. E. Almlöf, "A theoretical study of multidimensional nuclear tunneling in malonaldehyde," J. Chem. Phys. **91**, 4061–4072 (1989).

[11] Z. Smedarchina, W. Siebrand, and M. Z. Zgierski, "An instanton approach to intramolecular hydrogen exchange: Tunneling splittings in malonaldehyde and the hydrogenoxalate anion," J. Chem. Phys. **103**, 5326–5334 (1995).

[12] T. Baba, T. Tanaka, I. Morino, K. M. T. Yamada, and K. Tanaka, "Detection of the tunneling-rotation transitions of malonaldehyde in the submillimeter-wave region," J. Chem. Phys. **110**, 4131–4133 (1999).

[13] M. E. Tuckerman and D. Marx, "Heavy-atom skeleton quantization and proton tunneling in 'intermediate-barrier' hydrogen bonds," Phys. Rev. Lett. **86**, 4946–4949 (2001).

[14] A. C. P. Alves and J. M. Hollas, "The near ultra-violet spectrum of tropolone vapour and its relevance to the molecular structure," Mol. Phys. **23**, 927–945 (1972); "The near ultra-violet absorption spectrum of tropolone vapour II. Vibrational analysis," *ibid.* **25**, 1305–1314 (1973).

[15] R. L. Redington and T. E. Redington, "Tropolone monomer: Vibrational spectrum and proton tunneling," J. Mol. Spectrosc. **78**, 229–247 (1979).

[16] Y. Tomioka, M. Ito, and N. Mikami, "Electronic spectra of tropolone in a supersonic free jet. Proton tunneling in the S$_1$ state," J. Phys. Chem. **87**, 4401–4405 (1983).

[17] H. Sekiya, Y. Nagashima, and Y. Nishimura, "Electronic spectra of jet-cooled tropolone. Effect of the vibrational excitation on the proton tunneling dynamics," J. Chem. Phys. **92**, 5761–5769 (1990).

[18] S. Takada and H. Nakamura, "Effects of vibrational excitation on multidimensional tunneling: General study and proton tunneling in tropolone," J. Chem. Phys. **102**, 3977–3992 (1995).

[19] Z. Smedarchina, W. Siebrand, and M. Z. Zgierski, "Mode-specific hydrogen tunneling in tropolone: An instanton approach," J. Chem. Phys. **104**, 1203–1212 (1996).

[20] K. Tanaka, H. Honjo, T. Tanaka, H. Kohguchi, Y. Ohshima, and Y. Endo, "Determination of the proton tunneling splitting of tropolone in the ground state by microwave spectroscopy," J. Chem. Phys. **110**, 1969–1978 (1999).

[21] P. Liljeroth, J. Repp, and G. Meyer, "Current-induced hydrogen tautomerization and conductance switching of naphthalocyanine molecules," Science **317**, 1203–1206 (2007).

[22] A. Sperl, J. Kröger, and R. Berndt, "Controlled metalation of a single adsorbed phthalocyanine," Angew. Chem., Int. Ed. **50**, 5294–5297 (2011).

[23] W. Auwärter, K. Seufert, F. Bischoff, D. Ecija, S. Vijayaraghavan, S. Joshi, F. Klappenberger, N. Samudrala, and J. V. Barth, "A surface-anchored molecular four-level conductance switch based on single proton transfer," Nat. Nanotech. **7**, 41–46 (2012).

[24] J. Kügel, A. Sixta, M. Böhme, A. Krönlein, and M. Bode, "Breaking degeneracy of tautomerization—Metastability from days to seconds," ACS Nano **10**, 11058–11065 (2016).

[25] J. Kügel, M. Leisegang, M. Böhme, A. Krönlein, A. Sixta, and M. Bode, "Remote single-molecule switching: Identification and nanoengineering of hot electron-induced tautomerization," Nano Lett. **17**, 5106–5112 (2017).

[26] E. Vogel, M. Köcher, H. Schmickler, and J. Lex, "Porphycene—A novel porphin isomer," Angew. Chem., Int. Ed. **25**, 257–259 (1986).

[27] J. Waluk, "Spectroscopy and tautomerization studies of porphycenes," Chem. Rev. **117**, 2447–2480 (2017).

[28] P. Fita, L. Grill, A. Listkowski, H. Piwoński, S. Gawinkowski, M. Pszona, J. Sepioł, E. Mengesha, T. Kumagai, and J. Waluk, "Spectroscopic and microscopic investigations of tautomerization in porphycenes: Condensed phases, supersonic jets, and single molecule studies," Phys. Chem. Chem. Phys. **19**, 4921–4937 (2017).

[29] S. Gawinkowski, Ł. Walewski, A. Vdovin, A. Slenczka, S. Rols, M. R. Johnson, B. Lesyng, and J. Waluk, "Vibrations and hydrogen bonding in porphycene," Phys. Chem. Chem. Phys. **14**, 5489–5503 (2012).

[30] J. Waluk, "Ground- and excited-state tautomerism in porphycenes," Acc. Chem. Res. **39**, 945–952 (2006).

[31] P. Fita, N. Urbańska, C. Radzewicz, and J. Waluk, "Ground- and excited-state tautomerization rates in porphycenes," Chem. Eur. J. **15**, 4851–4856 (2009).

[32] M. Gil and J. Waluk, "Vibrational gating of double hydrogen tunneling in porphycene," J. Am. Chem. Soc. **129**, 1335–1341 (2007).

[33] A. Vdovin, J. Waluk, B. Dick, and A. Slenczka, "Mode-selective promotion and isotope effects of concerted double-hydrogen tunneling in porphycene embedded in superfluid helium nanodroplets," Chem. Phys. Chem. **10**, 761–765 (2009).

[34] P. Ciąćka, P. Fita, A. Listkowski, C. Radzewicz, and J. Waluk, "Evidence for dominant role of tunneling in condensed phases and at high temperatures: Double hydrogen transfer in porphycenes," J. Phys. Chem. Lett. **7**, 283–288 (2016).

[35] T. Kumagai, F. Hanke, S. Gawinkowski, J. Sharp, K. Kotsis, J. Waluk, M. Persson, and L. Grill, "Thermally and vibrationally induced tautomerization of single porphycene molecules on a Cu(110) surface," Phys. Rev. Lett. **111**, 246101 (2013).

[36] T. Kumagai, F. Hanke, S. Gawinkowski, J. Sharp, K. Kotsis, J. Waluk, M. Persson, and L. Grill, "Controlling intramolecular hydrogen transfer in a porphycene molecule with single atoms or molecules located nearby," Nat. Chem. **6**, 41–46 (2014).

[37] J. N. Ladenthin, L. Grill, S. Gawinkowski, Sh. Liu, J. Waluk, and T. Kumagai, "Hot carrier-induced tautomerization within a single porphycene molecule on Cu(111)," ACS Nano **9**, 7287–7295 (2015).

[38] H. Böckmann, S. Liu, J. Mielke, S. Gawinkowski, J. Waluk, L. Grill, M. Wolf, and T. Kumagai, "Direct observation of photoinduced tautomerization in single molecules at a metal surface," Nano Lett. **16**, 1034–1041 (2016).

[39] J. N. Ladenthin, T. Frederiksen, M. Persson, J. C. Sharp, S. Gawinkowski, J. Waluk, and T. Kumagai, "Force-induced tautomerization in a single molecule," Nat. Chem. **8**, 935–940 (2016).

[40] L. J. Lauhon and W. Ho, "Direct observation of the quantum tunnelling of single hydrogen atoms with a scanning tunnelling microscope," Phys. Rev. Lett. **85**, 4566–4569 (2000).

[41] T. Kumagai, M. Kaizu, S. Hatta, H. Okuyama, T. Aruga, I. Hamada, and Y. Morikawa, "Direct observation of hydrogen-bond exchange within a single water dimer," Phys. Rev. Lett. **100**, 166101 (2008).

[42] X. Meng, J. Guo, J. Peng, J. Chen, Z. Wang, J.-R. Shi, X.-Z. Li, E.-G. Wang, and Y. Jiang, "Direct visualization of concerted proton tunnelling in a water nanocluster," Nat. Phys. **11**, 235–239 (2015).

[43] M. Koch, M. Pagan, M. Persson, S. Gawinkowski, J. Waluk, and T. Kumagai, "Direct observation of double hydrogen transfer via quantum tunneling in a single porphycene molecule on a Ag(110) surface," J. Am. Chem. Soc. **139**, 12681–12687 (2017).

[44] T. Kumagai, M. Kaizu, H. Okuyama, S. Hatta, T. Aruga, I. Hamada, and Y. Morikawa, "Symmetric hydrogen bond in a water-hydroxyl complex on Cu(110)," Phys. Rev. B **81**, 045402 (2010).

[45] J. Guo, J.-T. Lü, Y. Feng, J. Chen, J. Peng, Z. Lin, X. Meng, Z. Wang, X.-Z. Li, E.-G. Wang, and Y. Jiang, "Nuclear quantum effects of hydrogen bonds probed by tip-enhanced inelastic electron tunneling," Science **352**, 321–325 (2016).

[46] J. Repp, S. Fölsch, G. Meyer, and K.-H. Rieder, "Site determination and thermally assisted tunneling in homogenous nucleation," Phys. Rev. Lett. **91**, 206102 (2003).

[47] J. A. Stroscio and R. J. Celotta, "Controlling the dynamics of a single atom in lateral atom manipulation," Science **306**, 242–247 (2004).

[48] A. J. Heinrich, C. P. Lutz, J. A. Gupta, and D. M. Eigler, "Molecule cascades," Science **298**, 1381–1387 (2002).

[49] V. Blum, R. Gehrke, F. Hanke, P. Havu, V. Havu, X. Ren, K. Reuter, and M. Scheffler, Comput. Phys. Commun. **180**, 2175 (2009).

[50] G. Kresse and J. Furthmüller, "Efficient iterative schemes for *ab initio* total-energy calculations using a plane-wave basis set," Phys. Rev. B **54**, 11169–11186 (1996).

[51] G. Kresse and D. Joubert, "From ultrasoft pseudopotentials to the projector augmented-wave method," Phys. Rev. B **59**, 1758–1775 (1999).

[52] M. Dion, H. Rydberg, E. Schröder, D. C. Langreth, and B. I. Lundqvist, "Van der Waals density functional for general geometries," Phys. Rev. Lett. **92**, 246401 (2004).

[53] G. Román-Pérez and J. M. Soler, "Efficient implementation of a van der Waals density functional: Application to double-wall carbon nanotubes," Phys. Rev. Lett. **103**, 096102 (2009).

[54] J. Klimeš, D. R. Bowler, and A. Michaelides, "Chemical accuracy for the van der Waals density functional," J. Phys.: Condens. Matter **22**, 022201 (2010).

[55] J. Klimeš, D. R. Bowler, and A. Michaelides, "Van der Waals density functionals applied to solids," Phys. Rev. B **83**, 195131 (2011).

[56] V. G. Ruiz, W. Liu, and A. Tkatchenko, "Density-functional theory with screened van der Waals interactions applied to atomic and molecular adsorbates on close-packed and non-close-packed surfaces," Phys. Rev. B **93**, 035118 (2016).

[57] J. Neugebauer and M. Scheffler, "Adsorbate-substrate and adsorbate-adsorbate interactions of Na and K adlayers on Al(111)," Phys. Rev. B **46**, 16067 (1992).

[58] G. Mills, H. Jónsson, and G. K. Schenter, "Reversible work transition state theory: Application to dissociative adsorption of hydrogen," Surf. Sci. **324**, 305–337 (1995).

[59] G. Henkelman, B. P. Uberuaga, and H. A. Jónsson, "A climbing image nudged elastic band method for finding saddle points and minimum energy paths," J. Chem. Phys. **113**, 9901–9904 (2000).

[60] J. Tersoff and D. R. Hamann, "Theory and application for the scanning tunneling microscope," Phys. Rev. Lett. **50**, 1998–2001 (1983).

[61] J. Tersoff and D. R. Hamann, "Theory of the scanning tunneling microscope," Phys. Rev. B **31**, 805–813 (1985).

[62] Y.-H. Zhang, P. Wahl, and K. Kern, "Quantum point contact microscopy," Nano Lett. **11**, 3838–3843 (2011).

[63] F. L. Hirshfeld, Theor. Chim. Acta **44**, 129 (1977).

[64] D. Novko, J. C. Tremblay, and M. Blanco-Rey, "On the tautomerisation of porphycene on copper (111): Finding the subtle balance between van der Waals interactions and hybridisation," J. Chem. Phys. **145**, 244701 (2016).

[65] D. Novko, J. C. Tremblay, and M. Blanco-Rey, "Erratum: 'On the tautomerisation of porphycene on copper (111): Finding the subtle balance between van der Waals interactions and hybridisation' [J. Chem. Phys. **145**, 244701 (2016)]," J. Chem. Phys. **147**, 169901 (2017).